Targeting STAT6 to mitigate sepsis-induced muscle atrophy and weakness: Modulation of mitochondrial dysfunction, ferroptosis, and CHI3L1-Mediated satellite cell loss

Zhiyong Sheng [a,b,c], Zhihong Yu [a,c], Meng Wang [a,c], Rui Zhou [b,c], Shenjian Chen [b,c], Xin Yu [a,c], Fuxing Li [a,c,*]

[a] *Department of Intensive Care Unit, The Second Affiliated Hospital of Nanchang University, Nanchang, 330006, Jiangxi, China*
[b] *Department of Neurological Intensive Care Unit, The Second Affiliated Hospital of Nanchang University, Nanchang, 330006, Jiangxi, China*
[c] *The Second Affiliated Hospital of Nanchang University, Nanchang, 330006, Jiangxi, China*

ARTICLE INFO

ABSTRACT

Sepsis-induced muscle weakness is a debilitating consequence of prolonged critical illness, often associated with a poor prognosis. While recent research has shown that STAT6 functions as an inhibitor of myogenesis, its role in sepsis-induced muscle weakness remains unclear. In this study, we hypothesized that inhibiting STAT6 could attenuate sepsis-induced muscle atrophy and weakness, and we explored the underlying mechanisms. Leveraging a microarray dataset from sepsis patients, we identified significant enrichment of genes related to muscle function, ferroptosis, and the p53 signalling pathway in muscle tissue from sepsis patients. Using a murine sepsis model induced by cecum ligation and puncture (CLP), we explore the multifaceted role of STAT6 inhibition. Our findings demonstrate that STAT6 inhibition effectively attenuates muscle atrophy, enhances grip strength, preserves mitochondrial integrity, and modulates ferroptosis in septic mice. Additionally, we identify elevated levels of CHI3L1 in septic muscle tissue, which are significantly reduced by STAT6 inhibition. In-depth analysis of primary muscle satellite cells reveals that CHI3L1 overexpression is associated with increased expression of key regulators of satellite cell myogenicity, while negatively impacting cell viability. Silencing CHI3L1 expression mitigates satellite cell injury and loss, highlighting its pivotal role in sepsis-induced muscle damage. In summary, this study unveils the potential of STAT6 as a therapeutic target for mitigating sepsis-induced muscle atrophy and weakness. Our findings underscore the regulation of mitochondrial dysfunction, ferroptosis, and CHI3L1-mediated satellite cell damage by STAT6, offering promising avenues for therapeutic intervention in the management of sepsis-induced muscle weakness.

1. Introduction

Sepsis, a life-threatening systemic response to infection, presents a complex and multifaceted challenge to the medical community. Over the years, advancements in medical treatments have led to a significant reduction in sepsis-related mortality rates, with a remarkable 53 % reduction observed from 1990 to 2017 [1]. However, sepsis remains a formidable adversary, causing not only immediate threats such as organ failure and shock but also leaving a trail of long-term consequences that profoundly impact patient outcomes. Among these consequences, sepsis-induced muscle weakness is an often-overlooked but critical issue. It is characterized by profound loss in muscle mass and quality, which

can amount to as much as 10–20 % within a week. In addition, muscle wasting resulting from sepsis has been associated with increased mortality and reduced quality of life for survivors [2].

Adult skeletal muscle possesses a remarkable capacity for regeneration, a process that comes into play in response to injury, disease, exercise, or the regular wear and tear [3]. This regenerative capacity depends on the presence of a specialized group of muscle stem cells, known as satellite cells (SCs), which are typically in a quiescent state and beneath the basal lamina and above the muscle sarcolemma of the muscle fibers [3]. However, upon muscle insults, signals originating from the altered microenvironment, or niche activate these SCs, and commit to proliferate and differentiation, initiating a cascade of

---

myogenic activity [4]. The activation and function of satellite cells are closely intertwined with the regenerative capacity of adult skeletal muscle. Impaired satellite cell function or a reduced number of satellite cells has been linked to various diseases and aging-related muscle decline [4–6].

Signal Transducer and Activator of Transcription 6 (STAT6) is renowned for its pivotal role in regulating immune responses, including the modulation of gene expression related to immunity, inflammation, and allergic reactions. However, its relevance extends beyond the realm of immunology. It has been indicated that STAT6 might function as an inhibitor of adult myogenesis, the process by which new muscle fibers are formed in mature organisms. This inhibition is achieved through the suppression of myogenin, a key regulator of muscle development. Moreover, it was observed that STAT6-deficient mice exhibited enhanced muscle regeneration following injury induced by cardiotoxin [7]. This suggests that STAT6 may exert a multifaceted influence, not solely confined to immune regulation, but also extending into the realms of muscle atrophy and dysfunction.

Ferroptosis, a distinctive form of regulated cell death characterized by iron-dependent lipid peroxidation, has gained prominence in various pathological conditions. Diverging from other classical programmed cell death pathways like apoptosis, necrosis, senescence, and autophagy, ferroptosis has unique morphological and biological characteristics. Recent evidence has underscored the role of ferroptosis in septic cardiomyopathy, marking it as a significant contributor to the pathogenesis of this condition [8–10]. Furthermore, ferroptosis has emerged as a formidable factor in skeletal muscle biology, impacting muscle cell death, proliferation, and differentiation [11]. For instance, research has revealed that the accumulation of labile iron in the skeletal muscles of aged rodents trigger ferroptosis, exacerbating age-related impairments in skeletal muscle regeneration [12].

Chitinase 3-like 1 (CHI3L1), a multifunctional glycoprotein, has been implicated in diverse inflammatory processes and is recognized for its potential role in muscle-related disorders [13–15]. Our previous study found that CHI3L1 was highly expressed in the skeletal muscle of septic mouse model, and inhibition of CHI3L1 dramatically alleviated skeletal muscle stem cell injury [15]. However, the interplay between STAT6, CHI3L1, and ferroptosis in sepsis-induced muscle weakness remains unclear. In this study, we explore the potential of inhibiting STAT6 as a means to mitigate sepsis-induced muscle weakness. Additionally, we investigate how STAT6 may modulate satellite cells and their susceptibility to ferroptosis, with CHI3L1 pathway as key mediators in this process. By shedding light on these intricate molecular mechanisms, our research aims to provide insights into innovative strategies to combat sepsis-induced muscle weakness, ultimately seeking to enhance the recovery and well-being of patients who face the enduring consequences of this condition.

2. Materials and methods

2.1. Ethics statement

Animal experiments were conducted under the approval of the Ethics Committee of the Second Affiliated Hospital of Nanchang University (Ethical Approval No. NCUFL-2021-10-29). The procedures for handling animals in this study were performed in strict accordance with the recommendations in the Guide for the Care and Use of Laboratory Animals.

2.2. Animal experiments

Eight-week-old Kunming mice (SWISS Mouse) were obtained from Spafford Biotechnology Ltd. (Beijing, China). All mice were group-housed (4 mice per cage) and had access to food and water ad libitum. They were kept in a pathogen-free environment with a 12-h light/dark cycle. To establish a sepsis model, we employed the cecum ligation and puncture (CLP) method, following established protocols [16]. In brief, mice were anesthetized with isoflurane, and the right abdomen was prepared by shaving. A 0.5-cm longitudinal incision was made to expose the cecum. The cecum was then ligated, and two perforations were created at the free end using a sterilized 18-gauge needle. Gentle pressure was applied to the cecum until a small amount of feces was expelled. Subsequently, the cecum was carefully repositioned within the abdominal cavity, and the incision was closed in two layers using a No. 4/0 suture. Sham mice underwent identical procedures to those in the CLP model group, with the sole exception being that they were neither ligated nor punctured. Age- and sex-matched controls were used in all experiments presented.

In the animal study, we randomized the subjects into 4 groups (n = 6 per group) and categorized them according to the following treatments: (i) Control group (Ctrl), (ii) Sham group (Sham), (iii) CLP model group (CLP), (iv) CLP + STAT6 inhibitor group (CLP + STAT6i). A previous study showed that intraperitoneal injection of AS1517499 at a dose of 10 mg/kg body weight effectively inhibited STAT6 activity in mice [17]. Therefore, in the CLP + STAT6i group model of this experiment, mice were intraperitoneally injected with AS1517499 (STAT6 inhibitor, 10 mg/kg; MedChemExpress, HY-100614) 1 h prior to establishing the CLP model. The various biological tissues from each group were collected 24 h after the CLP model was established for subsequent experiments. Additionally, we conducted daily monitoring of body weight and forelimb grip strength for one week after CLP modeling. Changes in muscle mass were assessed at 24 h and on day 7, respectively.

2.3. Body weight and forelimb grip strength test

Body weight and forelimb grip strength were assessed to evaluate the physical condition and skeletal muscle function in the experimental mice as described previously [18]. Forelimb grip strength was assessed using a digital Grip Strength Meter (GPM-100; Melquest, Toyama, Japan). The gauge was vertically oriented and secured to a metal stand to immobilize the system. Mice were allowed to grasp the bar, and an inspector gently pulled the tail of the mouse at a constant, slow speed. The peak pull force in grams was recorded using a digital force transducer. The first measurements of grip strength and body weight were performed before CLP modeling and then daily until day 7. Forelimb grip strength was normalized by body weight.

2.4. Muscle mass measurement

Muscle mass was assessed to evaluate the muscular changes in the experimental mice. The tibialis anterior (TA), gastrocnemius (GAS), and quadriceps (Quad) muscles of the mice were collected, frozen in liquid nitrogen, weighed, and then normalized by body weight.

2.5. Muscle satellite cells culture

Muscle satellite cells were purified and differentiated by differential adhesion as described in a previous study [15]. In short, skeletal muscles from 4-8-week-old Kunming mice were enzymatically digested with 0.2 % Collagenase II (Sigma-Aldrich, SCR103) at 37 °C for 1 h with agitation. The digestion was halted by adding Duchenne's Modified Eagle's Medium (DMEM, Gibco™ 11,965,092) with 10 % fetal bovine serum (FBS, Gibco™ A5209402, North America). After centrifugation of the muscle preparation and removing of the supernatant, a second digestion was performed using 0.25 % trypsin (Gibco™ 252,200,056) at 37 °C for 30 min with agitation. Subsequently, the digested cell suspensions were filtered through 70-μm cell strainer. Next, the cells were centrifuged, resuspended in DMEM supplemented with 20 % FBS, plated at a 60-mm culture dish, incubated in a 37 °C incubator with 5 % CO2. After 2 h, the non-adherent cells were transferred to a new culture dish and incubated for an additional 1 h at 37 °C in a 5 % CO2 incubator. The non-adherent cells were collected, centrifuged, counted, and resuspended in DMEM

with 20 % FBS, following the second pre-plating. The next day, plates containing various adherent muscle cells were rinsed three times with PBS. Subsequently, they were placed on ice for 15–30 min with occasional gentle manual shaking (swirling motion). The separated cells were collected, centrifuged, resuspended in growth media, and plated into 35-mm plates coated with 0.1 % gelatin (Sigma, 9000-70-8) at a density of 10^3 cells/dish. Finally, proliferating SCs were grown in differentiating media (DMEM containing 2 % horse serum) to induce differentiation.

2.6. Plasmids and small interfering RNA (siRNA) construction and transfection

Mouse CHI3L1 was amplified from mouse cDNA and ligated into pcDNA3.1 (+) vector at the *Bam*HI site by reverse-PCR to obtain the CHI3L1 expression plasmid. The expression of CHI3L1 was inhibited by siRNA interference. siRNA sequences were designed to specifically target CHI3L1. The antisense siRNA sequences were as follows (5′-3′): UUGCUGUAUCUGUCAAACCU (CHI3L1-siRNA).

The SCs were cultured until they reached 70–90 % confluence, and then transfected with pcDNA3.1 (+)-CHI3L1 overexpression vector, pcDNA™3.1/CAT control vector (Invitrogen™, V79020) and CHI3L1-siRNA, negative control siRNA (Invitrogen™, 4,390,843) using Lipofectamine 3000 Transfection Reagent (Invitrogen™, L3000001) according to the manufacturer's instructions. Briefly, two sterile EP tubes were acquired and loaded with 125 μl of Opti-MEM culture medium (Gibco™ 31,985,062) each. In one of these tubes, 5 μl of Lipofectamine 3000 Reagent was added, while the other tube received either 2.5 μg of plasmid (along with 5 μl of P3000) or 12.5 μl of siRNA (if in dry powder form, it was dissolved in 125 μl/OD). The solutions in the two tubes were mixed thoroughly. After an incubation period of 10–15 min, the mixtures were added to the SCs. Subsequently, Cells were incubated for 24 or 48 h (37 °C; 5 % CO2) and used for the following studies.

2.7. Cell treatments and in vitro grouping

To investigate the effects of CHI3L1 on SCs damage in septic environments, SCs were treated with lipopolysaccharide (LPS, Sigma-Aldrich) at 0.5, 1, 5, 10, 50, and 100 μg/ml for 24 h. Cell viability was assessed by CCK8 assay, and IL-1β levels in the culture medium were quantified by ELISA. The *in vitro* experiments were divided into 6 groups as follows: 1) control group (Con), 2) LPS group (5 μg/ml) (LPS), 3) LPS + pcDNA-CHI3L1 group (LPS + CHI3L1), 4) LPS + pcDNA control group (LPS + NC), 5) LPS + CHI3L1-siRNA group (LPS + CHI3L1-siRNA), 5) LPS + negative control siRNA (LPS + NC-siRNA). 48 h after transfection, SCs were treated with 5 μg/ml LPS for 24 h. Then the cells were collected to detect the levels of AKT, *P*-AKT and IL-1β with Western blot, and the supernatant was collected for Caspase-1 and IL-1β ELISA Assay.

2.8. Hematoxylin and eosin (H&E) staining

The skeletal muscle tissues were fixed in 4 % paraformaldehyde (PFA) for 24 h and then were sectioned into 5 μm slides. H&E staining were performed as previously described [19]. After the sections were deparaffinized, the sections were stained with hematoxylin to color cell nuclei blue-purple and eosin to stain cytoplasm and extracellular structures pink or red. After dehydration, clearing, and mounting with coverslips, the stained slides were observed under a microscope.

2.9. Immunohistochemistry (IHC)

The cell culture medium was aspirated, and the cells were washed twice with PBST. The cells were then fixed in a 4 % paraformaldehyde solution for 20 min, followed by three PBST washes to remove any residual fixative. The cells were blocked and permeabilized with a solution of PBS with 5 % normal goat serum and 0.1 % Triton X-100 for 2 h at

room temperature. Subsequently, SCs were incubated overnight at 4 °C with a primary antibody, Rabbit polyclonal to JAK1 (5 μg/ml, ab125051, Abcam), diluted in the blocking buffer. Afterwards, cells were rinsed twice with PBS and then washed three times with PBST. Next, primary antibody labled cells were incubated with a goat anti-rabbit IgG H&L secondary antibody (Alexa Fluor® 555) (1:500, ab150078, Abcam) for 2 h at room temperature while avoiding light. Following another round of PBS washing, the samples were mounted with Fluoroshield Mounting Medium with DAPI (ab104139, Abcam). Finally, the samples were observed and photographed using a confocal microscope.

2.10. Immunoblotting

Frozen skeletal muscle tissue or cultured SCs were homogenized on ice in RIPA buffer containing a protease inhibitor cocktail and phosphatase inhibitors (including 50 nM okadaic acid, 5 mM sodium pyrophosphate, and 50 mM NaF; Sigma-Aldrich). Protein levels of CHI3L1 and ferroptosis marker proteins, including Acyl-CoA synthetase long-chain family member 4 (ACSL4) (Abcam, ab155282), ferritin Heavy Chain 1 (FTH1) (Abcam, ab183781), glutathione peroxidase 4 (GPX4) (Abcam, ab252833), and Cyclooxygenases 2 (COX2) (Abcam, ab179800), were assessed in skeletal muscle tissue using quantitative Western blot analysis, following the protocols from our previous studies [15]. To investigate the impact of CHI3L1 on SCs injury, protein levels of interleukin-1β (IL-1β, Abcam, ab254360), phosphorylated and total protein kinase B (AKT, Cell signaling technology, #9272; *p*-AKT, Cell signaling technology, #4060) were examined in CHI3L1-siRNA transfected SCs following LPS treatment. Western blots were visualized using the ECL method (Thermo Scientific), and band intensities were quantified using Image J software. The protein level of each sample was calculated as the ratio of the target protein to GAPDH.

2.11. Quantitative PCR for analysis of gene transcripts

Total RNA was extracted from mouse skeletal muscle using the Ultrapure RNA Extraction Kit (D203-01, Beijing Genstar Biotechnology Co., Ltd.). The RNA was quantified and assessed for purity based on the A260/A280 ratio. Subsequently, 2 μg of total RNA was reverse transcribed to generate first-strand cDNA for real-time PCR. Reverse transcription was carried out using the Superscript II® Reverse Transcriptase Kit (Invitrogen) and random hexamer primers (Thermo Scientific). Reactions were incubated at 42 °C for 50 min and then at 90 °C for 5 min. Gene transcripts were quantified following established protocols [15]. Transcript levels of the Chi3l gene were determined using SYBR green binding technology with the following primers: forward primer, 5′-AGACGCCATCCAACCTTTCC-3′, reverse primer, 5′-GTTCGACTCGT-CATTCCACTC-3'. For delta-delta Ct analysis, GAPDH mRNA was used as an internal reference.

2.12. Cell counting kit-8 (CCK-8) assay

Cell proliferation was assessed following the instructions with the Cell Counting Kit-8 (HY–K0301, MedChemExpress). In brief, cells from various groups were washed with PBS, detached using trypsin, washed again with PBS, and resuspended. Cells were inoculated into 96-well plates at a density of 10×10^4 cells/μl and cultured in an incubator with 5 % CO2 at 37 °C for 24 h. Cells were then treated with LPS at concentrations of 0.5, 1, 5, 10, 50, and 100 μg/ml for 24 h. Following this treatment, 10 μl of CCK-8 solution was added to each well, and the plate was incubated for an additional 4 h in the incubator. The experiment was repeated 6 times, with 3 parallel wells established each time. Subsequently, the optical density (OD) values were measured at 450 nm using a microplate reader (UV-1800A, Shanghai Mercer Instrument Co., Ltd., Shanghai, China). The OD value for each well was calculated by subtracting the OD value of the blank group wells from the OD value of

the experimental wells.

2.13. Enzyme-linked immunosorbent assay (ELISA)

The levels of Caspase-1 and IL-1β in the culture medium of SCs were determined following the instructions provided with the mouse CASP1 ELISA kit (E-EL-M0201, Elabscience) and the IL-1 beta mouse ELISA kit (BMS6002, Invitrogen). In brief, the microwell strips were first washed, and standard dilutions were prepared. Then, the cell culture medium or prepared standard dilutions were added to the washed microwell strips. Biotin-Conjugate was added to all wells, and the mixture was incubated for 2 h at room temperature. After this incubation, the wells were washed four times and subsequently incubated with Streptavidin-HRP solution for 1 h at room temperature in the dark. Following another four washes, TMB Substrate Solution was added to all wells and incubated at room temperature for approximately 10 min. The enzyme reaction was stopped using Stop Solution. All samples were tested in duplicate, and the absorbance was measured at 620 nm using a microplate reader (UV-1800A, Shanghai Mercer Instrument Co., Ltd., Shanghai, China).

2.14. Transmission electron microscopy (TEM)

The muscle tissue was fixed in a 2.5 % glutaraldehyde buffer solution in 0.1 M cacodylate (pH 7.4) for a duration of 2 h. Subsequently, the tissue was thoroughly rinsed and then subjected to fixation in 1 % osmium tetroxide dissolved in 0.1 M cacodylate buffer, which lasted for approximately 2–3 h. Following another rinsing step, the tissue was systematically dehydrated through a graded series of solutions. After dehydration, the tissue was embedded and subsequently sectioned. To enhance visualization, a double staining procedure was performed involving 7.3 % acetic acid uranium and citric acid lead. The ultrastructural changes within the muscle tissue were meticulously examined under a transmission electron microscope.

2.15. Data collection

The data used in this study were sourced from the National Center for Biotechnology Information (NCBI) Gene Expression Omnibus (GEO) at https://www.ncbi.nlm.nih.gov/geo/. Specifically, microarray expression data from skeletal muscle tissues were extracted from GSE13205, comprising samples from 13 septic patients and 8 control patients [20].

2.16. Bioinformatics analysis

The Limma package was utilized to identify and screen for differentially expressed genes (DEGs) in the skeletal muscle tissues of 13 septic patients compared to 8 control patients [21]. We employed R packages such as ggplot 2 and Complex Heatmap to visualize these DEGs. Furthermore, we conducted Gene Set Enrichment Analysis (GSEA) using GSEA 4.3.2 to assess the potential skeletal muscle damage induced by sepsis. Additionally, GSEA was applied to validate functions related to iron toxicity in sepsis patients and explore possible signaling pathways involved in iron toxicity.

2.17. Statistical analysis

The data were presented as mean ± SD. To conduct multiple comparisons, we employed a one-way or two-way ANOVA of variance (ANOVA), followed by either the Bonferroni, Tukey, or Dunnett T3 post hoc test, depending on the results of Levene's test, which was used to assess the equality of variances among the groups. All statistical analyses were carried out using SPSS 21.0 statistical software (IBM Corp. Armonk, NY). Statistical significance was defined as $p < 0.05$.

3. Results

3.1. Inhibition of STAT6 attenuates sepsis-induced skeletal muscle atrophy

To investigate whether sepsis has a detrimental effect on skeletal muscle function and to identify potential underlying pathways, we conducted a reanalysis of the microarray dataset pertaining to skeletal muscle samples obtained from patients with sepsis and control subjects, originally collected by Olav Rooyackers and colleagues [20]. Bioinformatics analyses have revealed that skeletal muscle tissues from sepsis patients are enriched with genes associated with various muscular functions, including contractile fibers, myofibril, sarcomere, I-band, and Z-disc (Fig. 1A). Moreover, these genes are implicated in signaling pathways related to ferroptosis and the p53 signaling pathway (Fig. 1B).

In a murine model of sepsis induced by cecum ligation and puncture (CLP), we consistently observed a progressive reduction in body weight among the CLP mice over a 7-day period (Fig. 1C–D). Moreover, the mass of gastrocnemius (GAS) and quadriceps (Quad) skeletal muscles exhibited a significant decrease both at 24 h (Fig. 1E) and 7 days (Fig. 1F) after CLP induction. Although a statistically significant reduction in tibialis anterior (TA) muscle mass was noted only on day 7 post CLP induction (Fig. 1F), there was merely a declining trend observed at the 24-h mark following the establishment of CLP (Fig. 1E). These physical changes were in line with the observed reduction in forelimb grip strength in the CLP mice (Fig. 1G). Interestingly, our findings further revealed that treatment with the STAT6 inhibitor, AS1517499, had a significant mitigating effect on the reduction in body weight and skeletal muscle mass, as well as the decline in forelimb grip strength in CLP mice (Fig. 1D–G). Histological evidence from H&E staining further supported the favorable impact of STAT6 inhibition. As shown in Fig. 1H, the CLP model mice exhibited disorganized skeletal muscle structure and atrophied muscle fibers. In stark contrast, the group treated with the STAT6 inhibitor displayed tightly organized skeletal muscle fibers and indicated a marked improvement in skeletal muscle atrophy. Collectively, these findings suggest a pivotal role of STAT6 signaling in sepsis-induced skeletal muscle atrophy.

3.2. Inhibition of STAT6 reduces mitochondrial impairment in skeletal muscle of the CLP mouse model

Skeletal muscle mitochondrial malfunctions are found in septic patients during hospitalization in the intensive care unit, and this dysfunction is intricately linked to lean muscle performance [20,22]. To investigate whether the inhibition of STAT6 plays a role, at least in part, by mitigating the mitochondrial dysfunction associated with sepsis-induced skeletal muscle atrophy, we utilized transmission electron microscopy to assess the quadriceps mitochondrial structure 24 h after CLP modelling. In the Control and Sham groups, mitochondria displayed normal morphology, characterized by neat arrangement, intact membranes, undamaged and orderly skeletal muscle fibres, and clear intercalated discs and Z-lines. However, in the CLP group, mitochondrial organization was disrupted, with some mitochondria showing signs of swelling and degeneration. Additionally, some mitochondria became smaller and denser, while myofibers were fragmented, myofilament bundles detached, and the Z-lines became blurry. In contrast, the STAT6 inhibitor group demonstrated a notable reduction in mitochondrial damage compared to the CLP group. In this group, mitochondrial membranes remained more intact, and myofibrils were neatly arranged, indicating a mitigation of mitochondrial injury (Fig. 2). These findings suggest that inhibition of STAT6 may play a role in preserving mitochondrial function in sepsis-induced skeletal muscle atrophy.
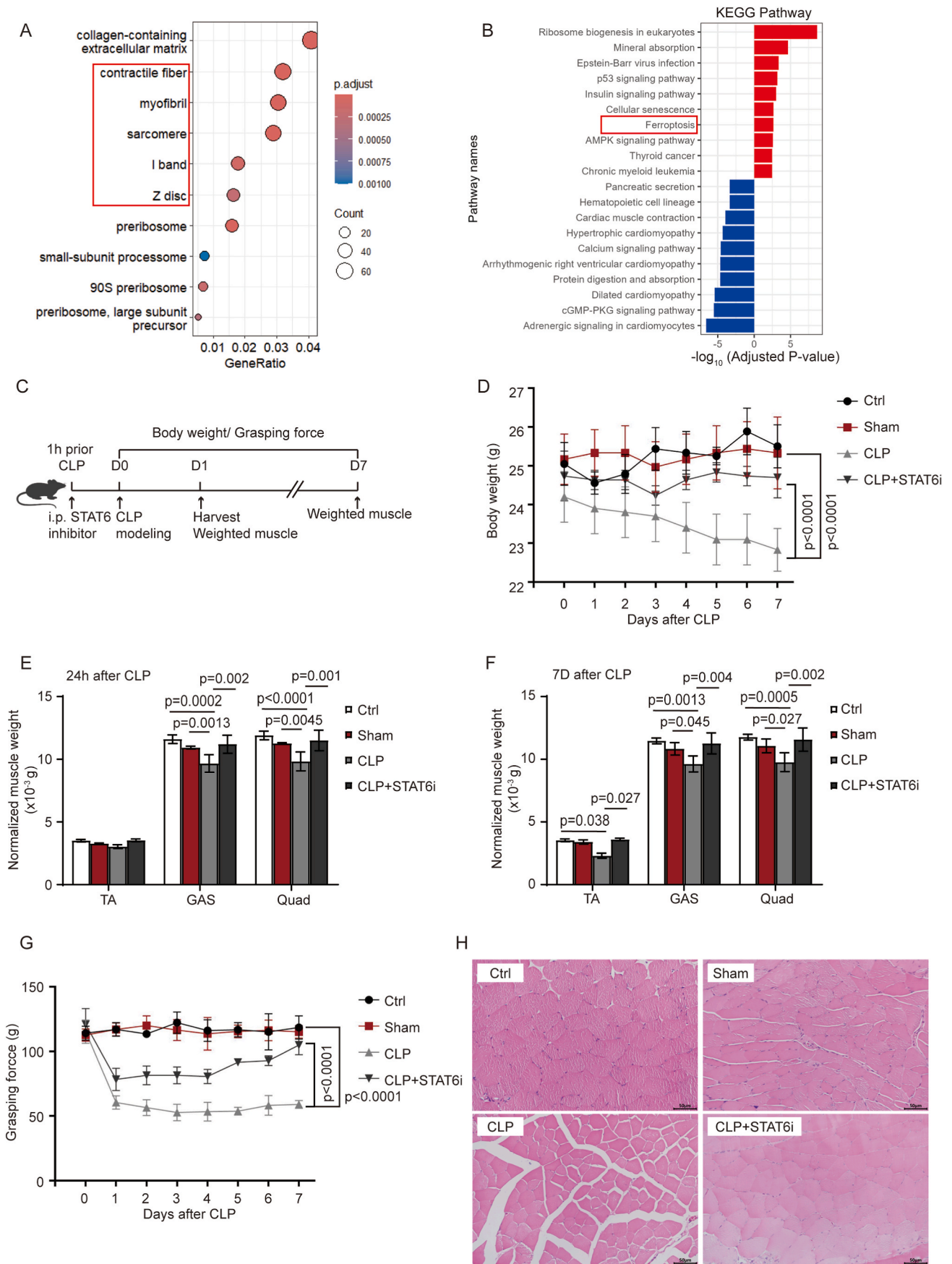
(caption on next page)

Fig. 1. Inhibition of STAT6 attenuates Sepsis-induced skeletal muscle atrophy. (A) Gene Ontology (GO) Analysis of Differentially Expressed Genes (DEGs) in Skeletal Muscle Tissues from Sepsis Patients: This panel displays the results of enrichment analysis for the top 10 GO terms in the Biological Process category. (B) Top 10 Significantly Upregulated and Downregulated KEGG Pathways in skeletal muscle tissues from sepsis patients. (C) Modeling and Experimentation Timeline. (D) Body Weight of Mice 7 Days after CLP Modeling. (*E*–*F*) Assessment of Tibialis Anterior (TA), Gastrocnemius (GAS), and Quadriceps (Quad) Muscle Mass at 24 h (E) and 7 Days (F) after CLP Modeling: This figure shows the measurements of muscle mass for the tibialis anterior, gastrocnemius, and quadriceps muscles 24 h post-CLP modeling. (G) Forelimb Grasping Force of Mice 7 Days after CLP Modeling. (H) Representative Photomicrograph of H&E Staining of Quadriceps Muscle Section (Scale bar 50 μm). All data are expressed as the mean ± SD, with n = 4 mice per group. For panels E and F, statistical analysis was performed using a one-way ANOVA, D and G was performed using a two-way ANOVA and p-values are displayed in the figure.
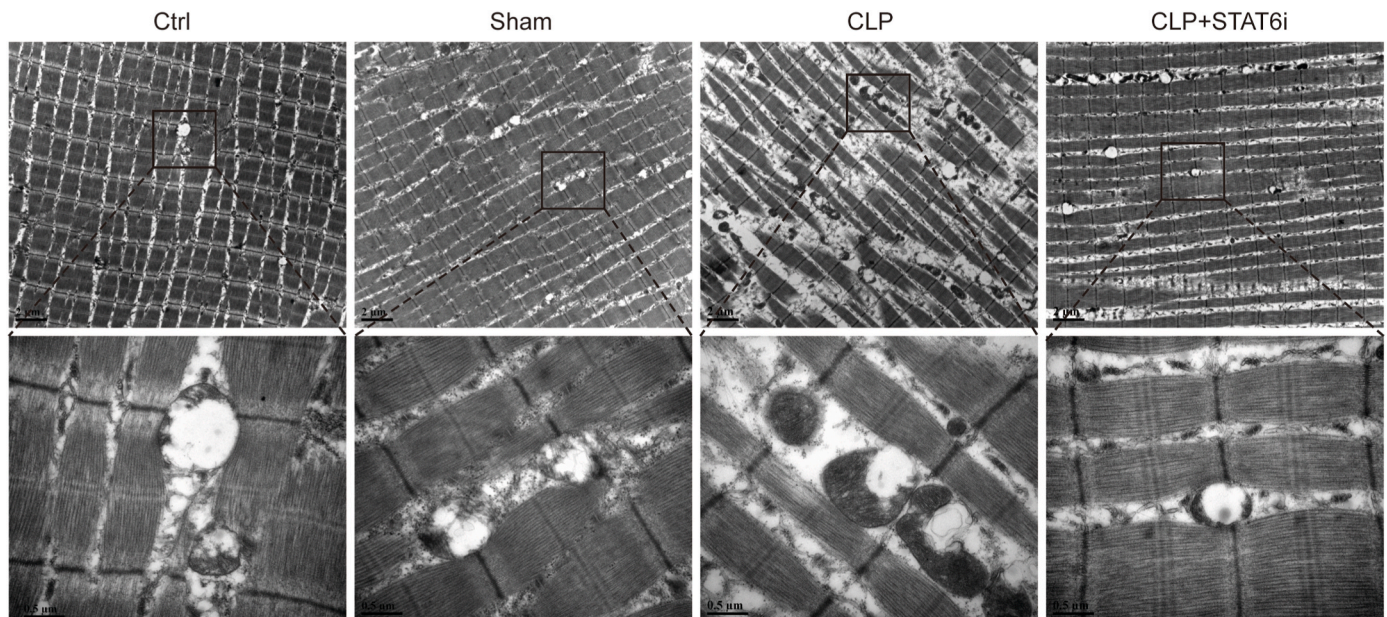

Fig. 2. Inhibition of STAT6 reduces mitochondrial impairment in skeletal muscle of the CLP mouse model. This figure presents a collection of representative images showcasing skeletal muscle fibers and mitochondrial morphology observed through transmission electron microscopy (TEM) in each of the experimental groups (First line, scale bar 2 μm). Additionally, a representative TEM micrograph of skeletal muscle is provided for each group, illustrating the morphology and abundance of mitochondria (Second line, scale bar 0.5 μm).

3.3. Inhibition of STAT6 protects against ferroptosis in skeletal muscle of the CLP mouse model

To delve deeper into the potential regulatory mechanisms underlying sepsis-induced skeletal muscle damage through mitochondrial dysfunction and ferroptosis, we conducted a comprehensive analysis. We specifically focused on ferroptosis- and mitochondrial-related proteins previously reported in the literature [23,24]. Through this analysis, we identified up-regulated differentially expressed genes (DEGs) in the skeletal muscles of sepsis patients. Intriguingly, our findings revealed that 105 of these up-regulated DEGs are concurrently associated with both mitochondrial dysfunction and ferroptosis, including ACSL4 and FTH1 (Fig. 3A). Subsequently, we collected quadriceps muscles from different groups of the CLP mouse model and extracted proteins for immunoblot analysis. The results showed a significant increase in the levels of ferroptosis marker proteins such as COX2, ACSL4, and FTH1 (Fig. 4B–E) in the quadriceps muscles of the CLP mouse model. Conversely, the inhibitor of ferroptosis, GPX4 (Fig. 4B, F), was notably decreased in the same muscle tissue. Interestingly, when we suppressed STAT6 activity, it not only reversed the CLP-induced elevation of COX2, ACSL4, and FTH1 but also ameliorated the reduction of GPX4 (Fig. 4B–F). These findings suggest that STAT6 signaling is intimately involved in sepsis-induced skeletal muscle damage through mechanisms related to mitochondrial dysfunction and ferroptosis.

3.4. Inhibition of STAT6 ameliorates skeletal muscle injury by reducing CHI3L1 mediated SCs damage

A total of 2115 genes (1275 up-regulated and 840 downregulated) were found to be significantly changed in the skeletal muscle of sepsis patients. These genes are labeled in the volcano map, with the top 5 most significantly elevated genes being SLPI, GLRX, MT1H, CHI3L1, and ERV3-2 (Fig. 4A). We also observed elevated levels of CHI3L1 in the quadriceps muscle of a sepsis mouse model (CLP), but this was reversed when we inhibited STAT6 (Fig. 4B). Our Gene Set Enrichment Analysis (GSEA) pointed towards a noteworthy association between sepsis-induced skeletal muscle damage and JAK-STAT signaling in the CLP mouse model (Fig. 4C). This is of particular interest given that primary muscle satellite cells highly express JAK1, and the JAK/STAT pathway has been reported to play a pivotal role in regulating myogenesis in adult satellite cells [25].

Expanding our investigation to muscle satellite cells, which play a pivotal role in muscle repair, we conducted experiments using primary satellite cells (Fig. 4D). These cells were exposed to varying concentrations of LPS to simulate the pathological conditions associated with sepsis. After evaluating both cell viability (Fig. 4E) and IL-1β levels in culture supernatants (Fig. 4F), we determined that a concentration of 5 μg/ml LPS were used in this study. Subsequently, we examined the effects of CHI3L1 manipulation. The introduction of the CHI3L1 plasmid significantly amplified the LPS-induced elevation of CHI3L1 transcription and protein expression (Fig. 5A, C). Conversely, the use of siRNA efficiently suppressed both CHI3L1 gene transcription and translation (Fig. 5B, D).
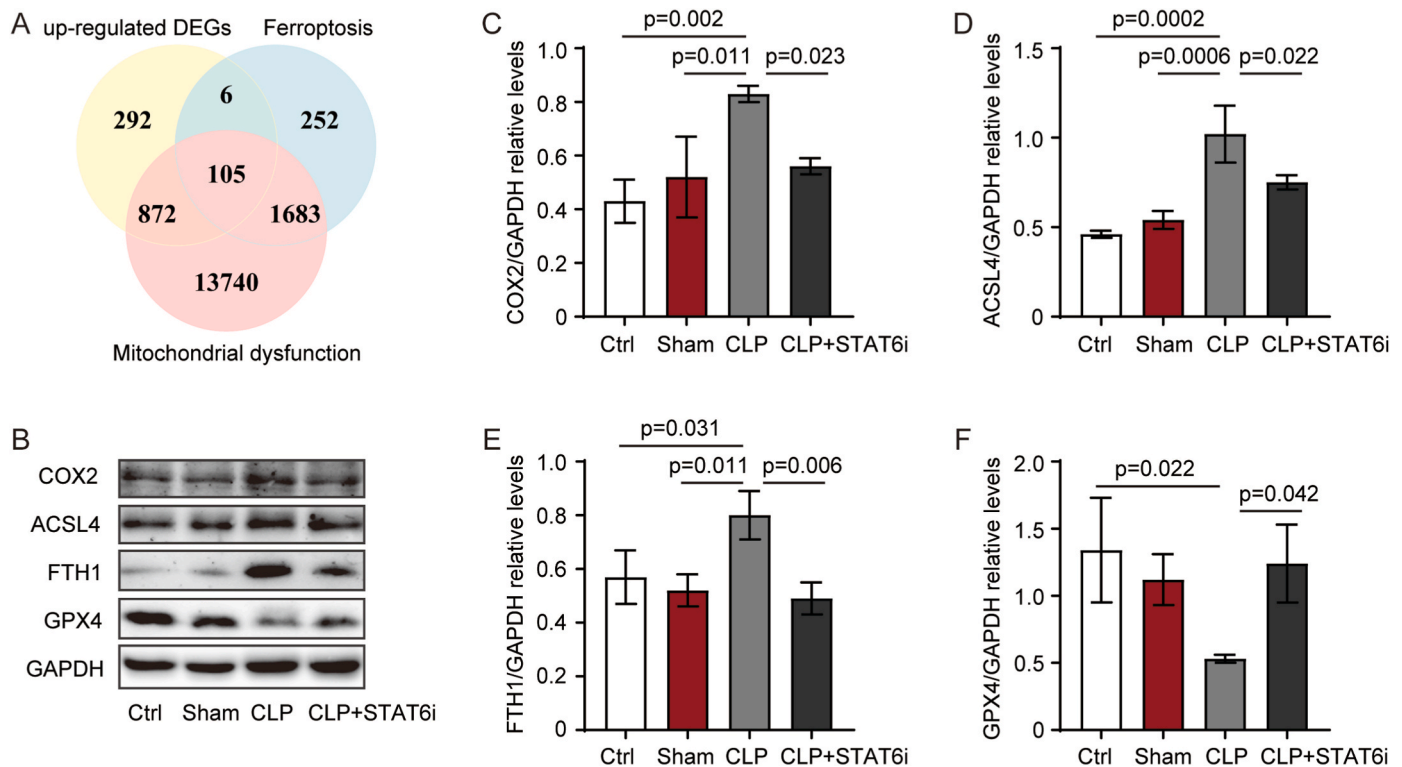
Fig. 3. Inhibition of STAT6 protects against ferroptosis in skeletal muscle of the CLP mouse model. (A) Venn diagrams illustrate an overlap of 105 genes among the 1275 up-regulated genes identified in skeletal muscle tissues from sepsis patients and those associated with mitochondrial dysfunction and ferroptosis (B) Representative Western blotting plots from skeletal muscle for each treatment group. (C–F) Relative expression levels of COX2 (C), ACSL4 (D), FTH1 (E), and GPX4 (F) for each group. All data are expressed as the mean ± SD, with n = 4 mice per group. Statistical analysis was conducted using a one-way ANOVA, and p-values are presented in the figure.

In our investigation of LPS-stimulated satellite cells, we observed a marked increase in the expression levels of IL-1β (Fig. 5E, H), which play pivotal roles in regulating satellite cell myogenicity. Simultaneously, there was a significant elevation in the phosphorylation level of AKT protein (Fig. 5E–G). Importantly, the results of our CHI3L1 over-expression experiments revealed a positive correlation between elevated CHI3L1 levels and increased expression of IL-1β, along with heightened AKT phosphorylation (Fig. 5E–H). Intriguingly, the elevation of CHI3L1 was inversely associated with cell viability (Fig. 5I). Conversely, when we silenced CHI3L1 expression, we observed a mitigation of satellite cell loss (Fig. 5I), coupled with the suppression of the upregulation of IL-1β (Fig. 5E, H) and AKT phosphorylation (Fig. 5E–G). Consistently, primary satellite cells that were overexpressing CHI3L1 showed a significant increase in the levels of IL-1β and Caspase1 in the culture supernatant following LPS stimulation (Fig. 5J and K). Importantly, this effect was reversed when we silenced CHI3L1 expression using CHI3L1 siRNA (Fig. 5J and K). These results highlight the direct influence of CHI3L1 on the secretion of pro-inflammatory cytokines, such as IL-1β, and the activation of Caspase1 in response to LPS stimulation in primary satellite cells. In conclusion, our results suggest that CHI3L1 could indeed modulate the function of satellite cells. Furthermore, STAT6 inhibitors may play a protective role in mitigating sepsis-induced skeletal muscle injury by down-regulating CHI3L1.

4. Discussion

Sepsis-induced muscle atrophy is a debilitating condition with a high prevalence in ICU patients [26]. This condition not only imposes a significant burden on the quality of life for survivors but also exerts substantial financial strain on the healthcare system due to prolonged hospitalization, specialized care requirements, and potential long-term rehabilitation needs [22]. Our study delved into the molecular

mechanisms of sepsis-induced muscle atrophy by analyzing a microarray dataset from sepsis patients. We identified a noteworthy enrichment of genes associated with various facets of muscle function in muscle tissue samples from sepsis patients. Notably, these enriched genes have substantial implications for iron metabolism and the p53 signaling pathway. Emerging evidence in the field has underscored the critical role of ferroptosis in the pathophysiology of sepsis-induced muscle atrophy [11]. Building upon this knowledge, our study investigated the potential therapeutic impact of inhibiting STAT6 in a murine model of sepsis induced CLP. We observed promising results, indicating that STAT6 inhibition could mitigate muscle atrophy, improve grip strength, and reduce mitochondrial impairment in CLP mice. Mechanistically, our findings suggest that STAT6 inhibition may confer protection against sepsis-induced skeletal muscle injury by modulating ferroptosis and mitigating CHI3L1-mediated injury to muscular satellite cells. These novel insights into the molecular mechanisms underlying sepsis-induced muscle atrophy could pave the way for the development of innovative therapies targeting STAT6 as a potential treatment strategy for sepsis-induced muscle atrophy.

STAT6, a transcription factor traditionally associated with immune regulation, particularly in type II immune responses, has recently been highlighted for its involvement in various pathophysiological events [27]. Research has demonstrated that interleukin-4, a T-cell cytokine, contributes to the suppression of cell-mediated immunity and sepsis-related mortality by acting through the STAT6 pathway [28]. Furthermore, STAT6-deficient (STAT6−/−) mice exhibit resistance to septic peritonitis, characterized by enhanced local bacterial clearance and the regulation of systemic organ damage [29]. Modulating STAT1 and STAT6 signals can influence macrophage polarization, thereby impacting survival and the severity of tissue damage in a septic mouse model [30]. These findings underscore the involvement of STAT6 in the immune-inflammatory response during sepsis. Echoing the results of a
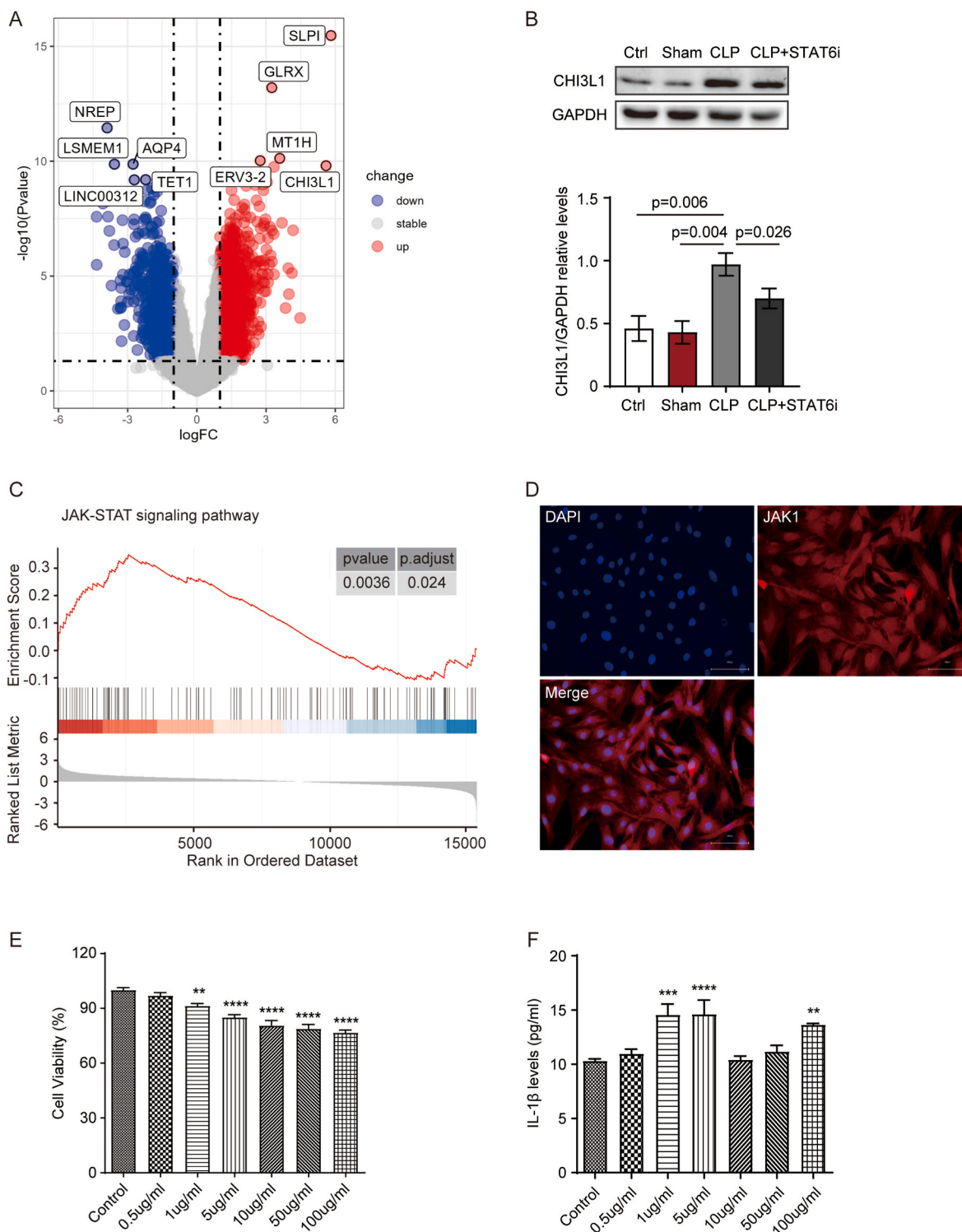
Fig. 4. Inhibition of STAT6 reduced CHI3L1 in skeletal muscle of septic group. (A) The volcano plot illustrates the differentially expressed genes in the skeletal muscle of septic patients compared to controls. It highlights the top five genes most significantly upregulated versus downregulated. (B) Western blot results demonstrate a substantial increase in skeletal muscle CHI3L1 levels in CLP mice, with downregulation of CHI3L1 levels observed following STAT6 inhibitor treatment (n = 4, one-way ANOVA, and p-values displayed in the figure). (C) A GSEA plot displays the enrichment of the "JAK-STAT signaling pathway" in the skeletal muscle of septic patients. (D) High expression of JAK1 is observed in primary cultured muscle satellite cells (Blue: DAPI, Red: JAK1). (E) Muscle satellite cells were exposed to various concentrations of LPS, and the LPS concentration used to mimic the septic environment was determined by evaluating cell viability using the CCK8 assay. (F) Levels of the inflammatory factor IL-1β in the culture medium supernatant were measured by ELISA (n = 4, one-way ANOVA, **p < 0.01, ***p < 0.001, ****p < 0.00001, Control vs. treatment). All data are expressed as the mean ± SD. (For interpretation of the references to color in this figure legend, the reader is referred to the Web version of this article.)
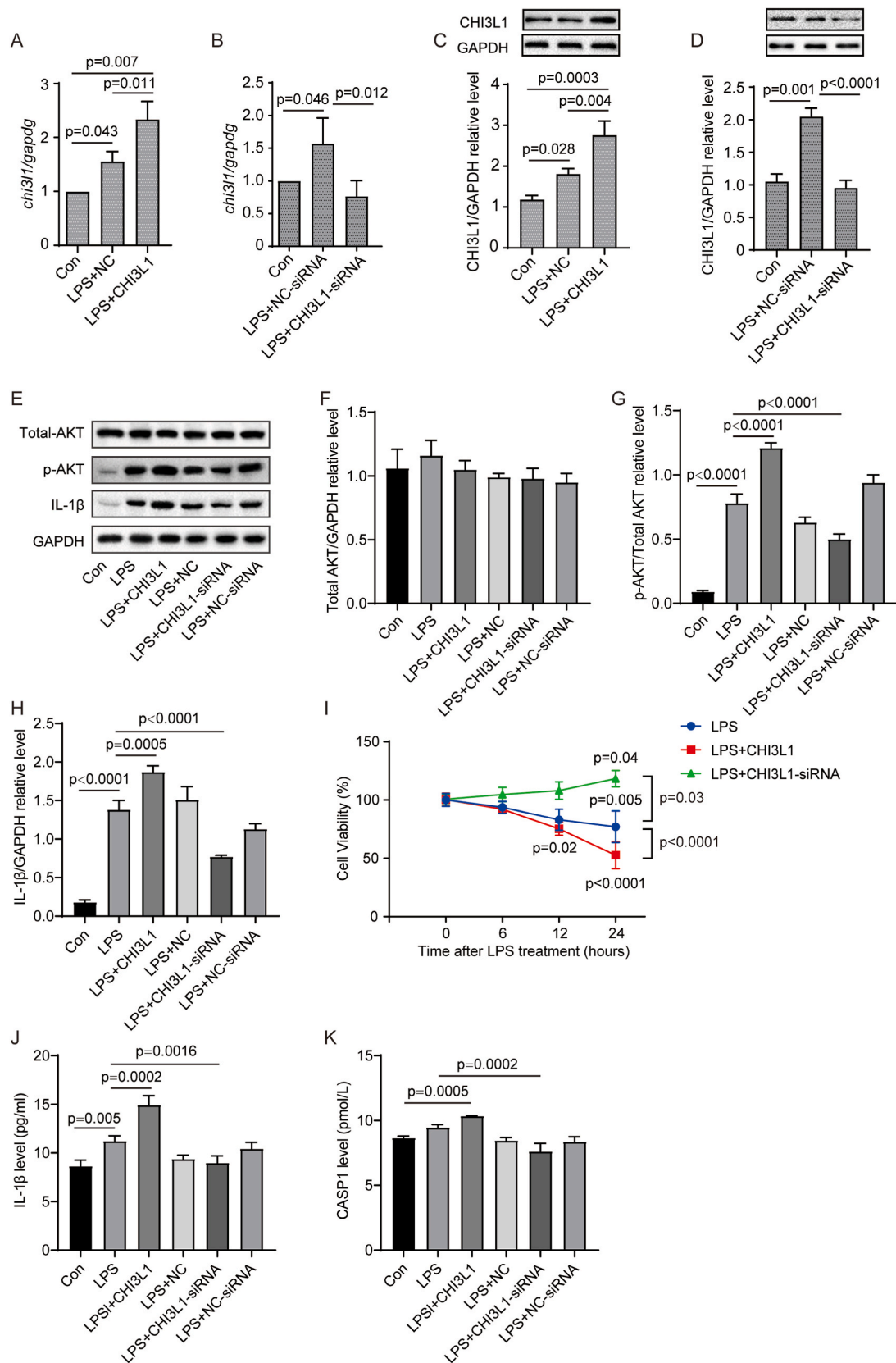
Fig. 5. Impact of CHI3L1 on Muscle Satellite Cells. (A, B) Relative levels of chi3l1 mRNA in pcDNA-CHI3L1 overexpressing and siRNA-CHI3L1 silencing muscle satellite cells after LPS treatment. (C, D) Western blot analysis of CHI3L1 in pcDNA-CHI3L1 overexpressing and siRNA-CHI3L1 silencing muscle satellite cells after LPS treatment. (E–H) Levels of IL-1β, total AKT, and phosphorylated p-AKT in CHI3L1 overexpression or silenced muscle satellite cells after LPS treatment. (I) CCK8 assay assessing the relationship between CHI3L1 and cell viability of muscle satellite cells. (J, K) Detection of the effect of CHI3L1 expression and silencing on IL-1β and Caspase1 (CASP1) levels in culture supernatants by ELISA. All data are expressed as the mean ± SD, n ≥ 3 per group. Statistical analyses used one-way ANOVA for all except for Fig. I, which was analyzed with two-way ANOVA. p-values are presented in the figure.

prior investigation conducted by Wong et al. [31], our research underscores the central role of STAT6 in muscle biology. Our results depict that treatment with the STAT6 inhibitor AS1517499 significantly mitigated the sepsis-induced reductions in body weight, skeletal muscle size, and grip strength. These outcomes underscore the critical involvement of STAT6 signalling in sepsis-induced skeletal muscle atrophy and highlight its potential therapeutic relevance for this condition. Beyond its well-established role in immune responses, STAT6 has garnered recognition for participating in tissue repair and regeneration processes, contributing to the healing and rejuvenation of damaged tissues. This expanded purview of STAT6's functions carries potential implications for understanding the mechanisms underlying muscle damage in sepsis.

The intricate regulation of skeletal muscle mass relies on a delicate balance between protein synthesis and protein breakdown rates. In 1964, mitochondrial dysfunction was first recognized as a catalyst for skeletal muscle atrophy. However, subsequent research unveiled a bidirectional relationship, indicating that mitochondrial dysfunction and skeletal muscle atrophy mutually exacerbate each other. The consequences of mitochondrial dysfunction extend beyond muscle wasting, triggering a cascade of detrimental events, including compromised energy production, heightened oxidative stress, ferroptosis induction, and protein turnover disruption. Recent research has shed light on the presence of STAT6 within mitochondria, suggesting a significant role for this transcription factor in mitochondrial biology and cellular oxidative metabolism [32–34]. Our study provides empirical evidence of the beneficial effects of STAT6 inhibition on mitochondrial integrity in CLP mice, highlighting the potential therapeutic role of STAT6 inhibition in ameliorating sepsis-induced skeletal muscle damage through the preservation of mitochondrial function.

Ferroptosis represents a novel form of programmed cell death that relies on iron-dependent mechanisms, distinct from classical programmed cell death pathways such as apoptosis, necroptosis, senescence, and autophagy. Mitochondria, central organelles responsible for iron metabolism and energy production, play a pivotal role in ferroptosis [35]. They act as the essential barrier against cellular demise, with characteristic morphological features including heightened mitochondrial membrane density, reduced mitochondrial volume compared to normal mitochondria, and outer mitochondrial membrane rupture [23]. Cells undergoing ferroptosis become immunogenic, potentially instigating a cascade of further cell death events and exacerbating the inflammatory response [36,37]. In our study, electron microscopy revealed ultrastructural characteristics in the CLP group, including smaller mitochondria, increased membrane density, reduced or absent cristae, and outer membrane rupture, providing additional evidence for iron-induced cell death in skeletal muscle cells of septic mice. Moreover, our comprehensive analysis identified a set of genes concurrently associated with mitochondrial dysfunction and ferroptosis in sepsis-affected skeletal muscles. This intriguing overlap suggests complex interactions between these pathways in sepsis-induced muscle damage.

Ferroptosis is indeed characterized by two major biochemical features: iron accumulation and lipid peroxidation. These features are closely interlinked and involve changes in the levels and activities of several essential proteins. Glutathione peroxidase 4 (GPX4) is a critical antioxidant enzyme and a central regulator in reducing lipid hydroperoxides and preventing lipid peroxidation. Inhibition or depletion of GPX4 results in its incapacity to reduce lipid peroxides, accumulating harmful lipid peroxides in cell membranes and ultimately triggering ferroptosis [38]. Studies in a mouse model of CLP have indicated that activation of the Nrf2/GPX4 signalling axis inhibits ferroptosis, thereby preventing sepsis-associated encephalopathy [39]. Our study reveals a substantial decrease in GPX4 expression in the skeletal muscles of septic mice, while STAT6 inhibition leads to an increase in GPX4 levels. Acyl-CoA synthetase long-chain family member 4 (ACSL4) enhances the presence of long-chain polyunsaturated ω6 fatty acids in cell membranes, rendering cells more susceptible to ferroptosis [40]. And ferritin heavy chain 1 (FTH1), a vital component of ferritin, can reduce intracellular free iron either by storing iron or binding with nuclear receptor coactivator 4 (NCOA4), facilitating ferritin degradation through iron autophagy. This process releases a substantial amount of iron, elevating cytoplasmic Fe^{2+} levels [11,23]. Consequently, this triggers the expression of mitochondrial transmembrane proteins, culminating in mitochondrial lipid peroxidation and cell death [24]. Our study observed elevated expression levels of ACSL4 and FTH1 in the CLP model group. Significantly, the administration of the STAT6 inhibitor resulted in a substantial reduction in the expression of both proteins. These findings underscore the intricate relationship between mitochondrial dysfunction and ferroptosis and the potential of STAT6 inhibition to modulate these pathways.

CHI3L1, also known as YKL-40, has emerged as a recognized biomarker for sepsis, demonstrating a positive correlation with disease severity [14,41]. Notably, CHI3L1 exerts a protective function by mitigating inflammation induced by TNFα and insulin resistance in skeletal muscles [42]. Additionally, research has indicated that exercise stimulates CHI3L1 production, fostering the proliferation of human muscle cells [13]. Recent studies have shed light on the association between acute skeletal muscle satellite cell injury during sepsis and mitochondrial dysfunction, potentially resulting in early and persistent impairments in satellite cell regeneration [26,43]. Our preliminary research findings suggest that CHI3L1 may exacerbate skeletal muscle tissue damage in septic mice. Interestingly, inhibiting CHI3L1 holds promise for enhancing satellite cell proliferation and suppressing apoptosis [15]. In the current study, we observed that elevated CHI3L1 expression correlated with increased expression of key regulators of satellite cell myogenicity, including IL-1β, and AKT phosphorylation, while inversely affecting cell viability. Silencing CHI3L1 expression attenuated Caspase-1 and IL-1β-mediated skeletal satellite cell injury and mitigated satellite cell loss. When synthesized with preceding research, these results suggest that STAT6 inhibitors, by down-regulating CHI3L1, may protect against sepsis-induced skeletal muscle injury. This insight opens avenues for further research into CHI3L1 as a potential therapeutic target.

In conclusion, this study provides compelling evidence regarding the molecular mechanisms involved in sepsis-induced muscle atrophy and potential therapeutic strategies to address this debilitating condition. Our results shed light on how STAT6 inhibition modulates mitochondrial function, ferroptosis, and CHI3L1 in sepsis-affected muscle damage. Encouragingly, inhibiting STAT6 in a murine sepsis model shows promise as a valuable therapeutic approach to mitigate muscle atrophy, enhance muscle strength, preserve mitochondrial function, and protect satellite cells. By unraveling these underlying molecular mechanisms and proposing potential therapeutic targets, this research paves the way for innovative treatment strategies that could improve patient outcomes and reduce the burden on healthcare systems. However, further research is essential to validate these findings and explore the safety and efficacy of STAT6-targeted therapies in clinical settings. Additionally, this study encourages continued investigations into the complex interactions between muscle biology, iron metabolism, and cell death pathways, as these insights could lead to more comprehensive approaches for managing sepsis-induced muscle atrophy.

Funding

Data availability statement

Our study has not generated new datasets.

CRediT authorship contribution statement

Zhiyong Sheng: Writing – original draft, Funding acquisition, Data curation, Conceptualization. **Zhihong Yu:** Writing – review & editing, Methodology. **Meng Wang:** Writing – review & editing, Resources. **Rui Zhou:** Writing – review & editing, Investigation. **Shenjian Chen:** Writing – review & editing, Investigation. **Xin Yu:** Writing – review & editing, Software. **Fuxing Li:** Writing – review & editing, Supervision, Resources, Funding acquisition, Formal analysis.

Declaration of competing interest

The authors declare that they have no known competing financial interests or personal relationships that could have appeared to influence the work reported in this paper.

Acknowledgments

References

[1] K.E. Rudd, S.C. Johnson, K.M. Agesa, K.A. Shackelford, D. Tsoi, D.R. Kievlan, D. V. Colombara, K.S. Ikuta, N. Kissoon, S. Finfer, C. Fleischmann-Struzek, F. R. Machado, K.K. Reinhart, K. Rowan, C.W. Seymour, R.S. Watson, T.E. West, F. Marinho, S.I. Hay, R. Lozano, A.D. Lopez, D.C. Angus, C.J.L. Murray, M. Naghavi, Global, regional, and national sepsis incidence and mortality, 1990-2017: analysis for the Global Burden of Disease Study, Lancet 395 (10219) (2020) 200–211, https://doi.org/10.1016/S0140-6736(19)32989-7.

[2] H.C. Prescott, D.C. Angus, Enhancing recovery from sepsis: a review, JAMA 319 (1) (2018) 62–75, https://doi.org/10.1001/jama.2017.17687.

[3] H. Yin, F. Price, M.A. Rudnicki, Satellite cells and the muscle stem cell niche, Physiol. Rev. 93 (1) (2013) 23–67, https://doi.org/10.1152/physrev.00043.2011.

[4] P. Sousa-Victor, L. Garcia-Prat, P. Munoz-Canoves, Control of satellite cell function in muscle regeneration and its disruption in ageing, Nat. Rev. Mol. Cell Biol. 23 (3) (2022) 204–226, https://doi.org/10.1038/s41580-021-00421-2.

[5] R.E. Schmitt, A. Dasgupta, P.C. Arneson-Wissink, S. Datta, A.M. Ducharme, J. D. Doles, Muscle stem cells contribute to long-term tissue repletion following surgical sepsis, J. Cachexia Sarcopenia Muscle 14 (3) (2023) 1424–1440, https://doi.org/10.1002/jcsm.13214.

[6] J.V. Chakkalakal, K.M. Jones, M.A. Basson, A.S. Brack, The aged niche disrupts muscle stem cell quiescence, Nature 490 (7420) (2012) 355–360, https://doi.org/10.1038/nature11438.

[7] M. Kurosaka, Y. Ogura, S. Sato, K. Kohda, T. Funabashi, Transcription factor signal transducer and activator of transcription 6 (STAT6) is an inhibitory factor for adult myogenesis, Skeletal Muscle 11 (1) (2021) 14, https://doi.org/10.1186/s13395-021-00271-8.

[8] N. Li, W. Wang, H. Zhou, Q. Wu, M. Duan, C. Liu, H. Wu, W. Deng, D. Shen, Q. Tang, Ferritinophagy-mediated ferroptosis is involved in sepsis-induced cardiac injury, Free Radic. Biol. Med. 160 (2020) 303–318, https://doi.org/10.1016/j.freeradbiomed.2020.08.009.

[9] C. Wang, W. Yuan, A. Hu, J. Lin, Z. Xia, C.F. Yang, Y. Li, Z. Zhang, Dexmedetomidine alleviated sepsis-induced myocardial ferroptosis and septic heart injury, Mol. Med. Rep. 22 (1) (2020) 175–184, https://doi.org/10.3892/mmr.2020.11114.

[10] X. Fang, H. Ardehali, J. Min, F. Wang, The molecular and metabolic landscape of iron and ferroptosis in cardiovascular disease, Nat. Rev. Cardiol. 20 (1) (2023) 7–23, https://doi.org/10.1038/s41569-022-00735-4.

[11] Y. Wang, Z. Zhang, W. Jiao, Y. Wang, X. Wang, Y. Zhao, X. Fan, L. Tian, X. Li, J. Mi, Ferroptosis and its role in skeletal muscle diseases, Front. Mol. Biosci. 9 (2022), 1051866, https://doi.org/10.3389/fmolb.2022.1051866.

[12] H. Ding, S. Chen, X. Pan, X. Dai, G. Pan, Z. Li, X. Mai, Y. Tian, S. Zhang, B. Liu, G. Cao, Z. Yao, X. Yao, L. Gao, L. Yang, X. Chen, J. Sun, H. Chen, M. Han, Y. Yin, G. Xu, H. Li, W. Wu, Z. Chen, J. Lin, L. Xiang, J. Hu, Y. Lu, X. Zhu, L. Xie, Transferrin receptor 1 ablation in satellite cells impedes skeletal muscle regeneration through activation of ferroptosis, J. Cachexia Sarcopenia Muscle 12 (3) (2021) 746–768, https://doi.org/10.1002/jcsm.12700.

[13] S.W. Gorgens, M. Hjorth, K. Eckardt, S. Wichert, F. Norheim, T. Holen, S. Lee, T. Langleite, K.I. Birkeland, H.K. Stadheim, K.J. Kolnes, D.S. Tangen, A.J. Kolnes, J. Jensen, C.A. Drevon, J. Eckel, The exercise-regulated myokine chitinase-3-like

[14] B. Kornblit, D. Hellemann, L. Munthe-Fog, J. Bonde, J.J. Strom, H.O. Madsen, J. S. Johansen, P. Garred, Plasma YKL-40 and CHI3L1 in systemic inflammation and sepsis-experience from two prospective cohorts, Immunobiology 218 (10) (2013) 1227–1234, https://doi.org/10.1016/j.imbio.2013.04.010.

[15] F. Li, Z. Sheng, H. Lan, J. Xu, J. Li, Downregulated CHI3L1 alleviates skeletal muscle stem cell injury in a mouse model of sepsis, IUBMB Life 72 (2) (2020) 214–225, https://doi.org/10.1002/iub.2156.

[16] J.A. Buras, B. Holzmann, M. Sitkovsky, Animal models of sepsis: setting the stage, Nat. Rev. Drug Discov. 4 (10) (2005) 854–865, https://doi.org/10.1038/nrd1854.

[17] Y. Chiba, M. Todoroki, Y. Nishida, M. Tanabe, M. Misawa, A novel STAT6 inhibitor AS1517499 ameliorates antigen-induced bronchial hypercontractility in mice, Am. J. Respir. Cell Mol. Biol. 41 (5) (2009) 516–524, https://doi.org/10.1165/rcmb.2008-0163OC.

[18] H. Takeshita, K. Yamamoto, S. Nozato, T. Inagaki, H. Tsuchimochi, M. Shirai, R. Yamamoto, Y. Imaizumi, K. Hongyo, S. Yokoyama, M. Takeda, R. Oguro, Y. Takami, N. Itoh, Y. Takeya, K. Sugimoto, S.I. Fukada, H. Rakugi, Modified forelimb grip strength test detects aging-associated physiological decline in skeletal muscle function in male mice, Sci. Rep. 7 (2017), 42323, https://doi.org/10.1038/srep42323.

[19] C. Wang, F. Yue, S. Kuang, Muscle histology characterization using H&E staining and muscle fiber type classification using immunofluorescence staining, Bio. Protoc. 7 (10) (2017), https://doi.org/10.21769/BioProtoc.2279.

[20] K. Fredriksson, I. Tjader, P. Keller, N. Petrovic, B. Ahlman, C. Scheele, J. Wernerman, J.A. Timmons, O. Rooyackers, Dysregulation of mitochondrial dynamics and the muscle transcriptome in ICU patients suffering from sepsis induced multiple organ failure, PLoS One 3 (11) (2008) e3686, https://doi.org/10.1371/journal.pone.0003686.

[21] J. Reimand, R. Isserlin, V. Voisin, M. Kucera, C. Tannus-Lopes, A. Rostamianfar, L. Wadi, M. Meyer, J. Wong, C. Xu, D. Merico, G.D. Bader, Pathway enrichment analysis and visualization of omics data using g:Profiler, GSEA, Cytoscape and EnrichmentMap, Nat. Protoc. 14 (2) (2019) 482–517, https://doi.org/10.1038/s41596-018-0103-9.

[22] A.M. Owen, S.P. Patel, J.D. Smith, B.K. Balasuriya, S.F. Mori, G.S. Hawk, A. J. Stromberg, N. Kuriyama, M. Kaneki, A.G. Rabchevsky, T.A. Butterfield, K. A. Esser, C.A. Peterson, M.E. Starr, H. Saito, Chronic muscle weakness and mitochondrial dysfunction in the absence of sustained atrophy in a preclinical sepsis model, Elife (2019), https://doi.org/10.7554/eLife.49920.

[23] X. Jiang, B.R. Stockwell, M. Conrad, Ferroptosis: mechanisms, biology and role in disease, Nat. Rev. Mol. Cell Biol. 22 (4) (2021) 266–282, https://doi.org/10.1038/s41580-020-00324-8.

[24] H. Wang, C. Liu, Y. Zhao, G. Gao, Mitochondria regulation in ferroptosis, Eur. J. Cell Biol. 99 (1) (2020), 151058, https://doi.org/10.1016/j.ejcb.2019.151058.

[25] L. Zanders, M. Kny, A. Hahn, S. Schmidt, S. Wundersitz, M. Todiras, I. Lahmann, A. Bandyopadhyay, T. Wollersheim, L. Kaderali, F.C. Luft, C. Birchmeier, S. Weber-Carstens, J. Fielitz, Sepsis induces interleukin 6, gp130/JAK2/STAT3, and muscle wasting, J. Cachexia Sarcopenia Muscle 13 (1) (2022) 713–727, https://doi.org/10.1002/jcsm.12867.

[26] P. Rocheteau, L. Chatre, D. Briand, M. Mebarki, G. Jouvion, J. Bardon, C. Crochemore, P. Serrani, P.P. Lecci, M. Latil, B. Matot, P.G. Carlier, N. Latronico, C. Huchet, A. Lafoux, T. Sharshar, M. Ricchetti, F. Chretien, Sepsis induces long-term metabolic and mitochondrial muscle stem cell dysfunction amenable by mesenchymal stem cell therapy, Nat. Commun. 6 (2015), 10145, https://doi.org/10.1038/ncomms10145.

[27] S. Goenka, M.H. Kaplan, Transcriptional regulation by STAT6, Immunol. Res. 50 (1) (2011) 87–96, https://doi.org/10.1007/s12026-011-8205-2.

[28] G.Y. Song, C.S. Chung, I.H. Chaudry, A. Ayala, IL-4-induced activation of the Stat6 pathway contributes to the suppression of cell-mediated immunity and death in sepsis, Surgery 128 (2) (2000) 133–138, https://doi.org/10.1067/msy.2000.107282.

[29] A. Matsukawa, M.H. Kaplan, C.M. Hogaboam, N.W. Lukacs, S.L. Kunkel, Pivotal role of signal transducer and activator of transcription (Stat)4 and Stat6 in the innate immune response during sepsis, J. Exp. Med. 193 (6) (2001) 679–688, https://doi.org/10.1084/jem.193.6.679.

[30] L. Feng, P. Song, H. Zhou, A. Li, Y. Ma, X. Zhang, H. Liu, G. Xu, Y. Zhou, X. Wu, Y. Shen, Y. Sun, X. Wu, Q. Xu, Pentamethoxyflavanone regulates macrophage polarization and ameliorates sepsis in mice, Biochem. Pharmacol. 89 (1) (2014) 109–118, https://doi.org/10.1016/j.bcp.2014.02.016.

[31] H. Li, C. He, R. Zhu, F.M. Chen, L. Wang, F.P. Leung, X.Y. Tian, G. Tse, W.T. Wong, Type 2 cytokines promote angiogenesis in ischemic muscle via endothelial IL-4Ralpha signaling, Cell Rep. 42 (8) (2023), 112964, https://doi.org/10.1016/j.celrep.2023.112964.

[32] P. Su, Q. Wang, E. Bi, X. Ma, L. Liu, M. Yang, J. Qian, Q. Yi, Enhanced lipid accumulation and metabolism are required for the differentiation and activation of tumor-associated macrophages, Cancer Res. 80 (7) (2020) 1438–1450, https://doi.org/10.1158/0008-5472.CAN-19-2994.

[33] D. Vats, L. Mukundan, J.I. Odegaard, L. Zhang, K.L. Smith, C.R. Morel, R. A. Wagner, D.R. Greaves, P.J. Murray, A. Chawla, Oxidative metabolism and PGC-1 beta attenuate macrophage-mediated inflammation, Cell Metabol. 4 (1) (2006) 13–24, https://doi.org/10.1016/j.cmet.2006.05.011.

[34] J.A. Meier, A.C. Larner, Toward a new STATe: the role of STATs in mitochondrial function, Semin. Immunol. 26 (1) (2014) 20–28, https://doi.org/10.1016/j.smim.2013.12.005.

[35] M. Gao, J. Yi, J. Zhu, A.M. Minikes, P. Monian, C.B. Thompson, X. Jiang, Role of mitochondria in ferroptosis, Mol. Cell 73 (2) (2019) 354–363 e3, https://doi.org/10.1016/j.molcel.2018.10.042.

[36] D. Martin-Sanchez, O. Ruiz-Andres, J. Poveda, S. Carrasco, P. Cannata-Ortiz, M. D. Sanchez-Nino, M. Ruiz Ortega, J. Egido, A. Linkermann, A. Ortiz, A.B. Sanz, Ferroptosis, but not necroptosis, is important in nephrotoxic folic acid-induced AKI, J. Am. Soc. Nephrol. 28 (1) (2017) 218–229, https://doi.org/10.1681/ASN.2015121376.

[37] B.R. Stockwell, Emerging mechanisms, physiological functions, and therapeutic applications, Cell 185 (14) (2022) 2401–2421, https://doi.org/10.1016/j.cell.2022.06.003.

[38] X. Chen, R. Kang, G. Kroemer, D. Tang, Ferroptosis in infection, inflammation, and immunity, J. Exp. Med. 218 (6) (2021), https://doi.org/10.1084/jem.20210518.

[39] J. Wang, Q. Zhu, Y. Wang, J. Peng, L. Shao, X. Li, Irisin protects against sepsis-associated encephalopathy by suppressing ferroptosis via activation of the Nrf2/GPX4 signal axis, Free Radic. Biol. Med. 187 (2022) 171–184, https://doi.org/10.1016/j.freeradbiomed.2022.05.023.

[40] S. Doll, B. Proneth, Y.Y. Tyurina, E. Panzilius, S. Kobayashi, I. Ingold, M. Irmler, J. Beckers, M. Aichler, A. Walch, H. Prokisch, D. Trumbach, G. Mao, F. Qu, H. Bayir, J. Fullekrug, C.H. Scheel, W. Wurst, J.A. Schick, V.E. Kagan, J.P. Angeli, M. Conrad, ACSL4 dictates ferroptosis sensitivity by shaping cellular lipid composition, Nat. Chem. Biol. 13 (1) (2017) 91–98, https://doi.org/10.1038/nchembio.2239.

[41] N. Hattori, S. Oda, T. Sadahiro, M. Nakamura, R. Abe, K. Shinozaki, F. Nomura, T. Tomonaga, K. Matsushita, Y. Kodera, K. Sogawa, M. Satoh, H. Hirasawa, YKL-40 identified by proteomic analysis as a biomarker of sepsis, Shock 32 (4) (2009) 393–400, https://doi.org/10.1097/SHK.0b013e31819e2c0c.

[42] S.W. Gorgens, K. Eckardt, M. Elsen, N. Tennagels, J. Eckel, Chitinase-3-like protein 1 protects skeletal muscle from TNFalpha-induced inflammation and insulin resistance, Biochem. J. 459 (3) (2014) 479–488, https://doi.org/10.1042/BJ20131151.

[43] L. Chatre, F. Verdonk, P. Rocheteau, C. Crochemore, F. Chretien, M. Ricchetti, A novel paradigm links mitochondrial dysfunction with muscle stem cell impairment in sepsis, Biochim. Biophys. Acta, Mol. Basis Dis. 1863 (10 Pt B) (2017) 2546–2553, https://doi.org/10.1016/j.bbadis.2017.04.019.